



Published in final edited form as:

Calcif Tissue Int. 2012 March ; 90(3): 202–210. doi:10.1007/s00223-012-9570-0.

Bisphosphonate Binding Affinity Affects Drug Distribution in Both Intracortical and Trabecular Bone of Rabbits

John Turek,

Department of Basic Medical Sciences, Purdue University, West Lafayette, IN, USA

Department of Anatomy and Cell Biology, Indiana University School of Medicine, 635 Barnhill Dr., MS 5035, Indianapolis, IN 46202, USA

F. Hal Ebetino,

Warner-Chilcott, Dundalk, Co Louth, Ireland

Mark W. Lundy,

Department of Anatomy and Cell Biology, Indiana University School of Medicine, 635 Barnhill Dr., MS 5035, Indianapolis, IN 46202, USA

Shuting Sun,

Department of Chemistry, University of Southern California, Los Angeles, CA, USA

Boris A. Kashemirov,

Department of Chemistry, University of Southern California, Los Angeles, CA, USA

Charles E. McKenna,

Department of Chemistry, University of Southern California, Los Angeles, CA, USA

Maxime A. Gallant,

Department of Anatomy and Cell Biology, Indiana University School of Medicine, 635 Barnhill Dr., MS 5035, Indianapolis, IN 46202, USA

Lilian I. Plotkin,

Department of Anatomy and Cell Biology, Indiana University School of Medicine, 635 Barnhill Dr., MS 5035, Indianapolis, IN 46202, USA

Teresita Bellido,

Department of Anatomy and Cell Biology, Indiana University School of Medicine, 635 Barnhill Dr., MS 5035, Indianapolis, IN 46202, USA

Xuchen Duan,

Nuffield Department of Orthopaedics, Rheumatology & Musculoskeletal Sciences, Nuffield Orthopaedic Centre, Oxford University Institute of Musculoskeletal Sciences, Headington, Oxford OX3 7LD, UK

✉ matallen@iupui.edu .

M. Allen has received funding from Warner Chilcott. D. Burr has received remuneration from Eli Lilly and Amgen; serves as consultant for Eli Lilly, Procter and Gamble, Amgen, and PharmaLegacy; and has received funding from Eli Lilly, Procter and Gamble, Pfizer, NephroGenex, The Alliance for Better Bone Health, and Amgen. C. McKenna, M. Lundy, and G. Russell have had consultant/advisory roles to Warner Chilcott. F. Ebetino is an employee of Warner Chilcott. All other authors have stated that they have no conflict of interest.

James T. Triffitt,

Nuffield Department of Orthopaedics, Rheumatology & Musculoskeletal Sciences, Nuffield Orthopaedic Centre, Oxford University Institute of Musculoskeletal Sciences, Headington, Oxford OX3 7LD, UK

R. Graham G. Russell,

Nuffield Department of Orthopaedics, Rheumatology & Musculoskeletal Sciences, Nuffield Orthopaedic Centre, Oxford University Institute of Musculoskeletal Sciences, Headington, Oxford OX3 7LD, UK

David B. Burr,

Department of Anatomy and Cell Biology, Indiana University School of Medicine, 635 Barnhill Dr., MS 5035, Indianapolis, IN 46202, USA

Matthew R. Allen

Department of Anatomy and Cell Biology, Indiana University School of Medicine, 635 Barnhill Dr., MS 5035, Indianapolis, IN 46202, USA

Abstract

Differences in the binding affinities of bisphosphonates for bone mineral have been proposed to determine their localizations and duration of action within bone. The main objective of this study was to test the hypothesis that mineral binding affinity affects bisphosphonate distribution at the basic multicellular unit (BMU) level within both cortical and cancellous bone. To accomplish this objective, skeletally mature female rabbits ($n = 8$) were injected simultaneously with both low- and high-affinity bisphosphonate analogs bound to different fluorophores. Skeletal distribution was assessed in the rib, tibia, and vertebra using confocal microscopy. The staining intensity ratio between osteocytes contained within the cement line of newly formed rib osteons or within the reversal line of hemiosteons in vertebral trabeculae compared to osteocytes outside the cement/reversal line was greater for the high-affinity compared to the low-affinity compound. This indicates that the low-affinity compound distributes more equally across the cement/reversal line compared to a high-affinity compound, which concentrates mostly near surfaces. These data, from an animal model that undergoes intracortical remodeling similar to humans, demonstrate that the affinity of bisphosphonates for the bone determines the reach of the drugs in both cortical and cancellous bone.

Keywords

Anti-remodeling; Skeletal distribution; Drug accumulation; Fluorescent bisphosphonate

Introduction

All bisphosphonates have a common P-C-P backbone yet vary with respect to their two side groups. Differences in these side chains affect both the potency of osteoclast enzyme inhibition and the binding affinity to bone mineral [1–3]. Binding affinity has been suggested to play a key role in a number of clinically important effects including the

speed of onset for fracture reduction, the recovery of bone turnover following treatment withdrawal, and differences in fracture risk reduction across skeletal sites [3].

Binding affinity determines the strength of drug attachment to mineral, yet it also affects where the drug is distributed throughout the skeleton. Upon exiting the vasculature, bisphosphonates will move through nonmineralized space and become bound to any mineral they encounter. Using radiolabeled [4] or fluorescent [5–9] bisphosphonates, studies have documented binding of drug to trabecular and endocortical bone surfaces, vascular channels, and osteocyte lacunae. Compared with radioactive labeling, the new fluorescent imaging probes derived from modern clinical nitrogen-containing bisphosphonates such as risedronate (RIS) offer important advantages of convenience, safety, resolution, sensitivity, and versatility [10]. Near-infrared fluorescent dyes can be applied in this approach to create imaging probes with emission wavelengths of 600–1,000 nm. These are ideal tools for in vivo imaging because autofluorescence from the tissues is minimized in this optical window [11]. Using such fluorescently labeled bisphosphonates that possess different binding affinities, it has been demonstrated that drugs with lower affinity penetrate deeper into the matrix at the trabecular or endocortical surfaces relative to those with higher affinities [7–9]. These data suggest that agents with lower binding affinity may have greater access to the osteocyte – canalicular network compared to higher-affinity compounds. As bisphosphonates attenuate osteocyte apoptosis [12, 13], this differential distribution could influence their pharmacological actions.

The main objective of this study was to test the hypothesis that mineral binding affinity affects bisphosphonate distribution at the basic multicellular unit (BMU) level within either cortical or cancellous bone. To accomplish this objective, skeletally mature female rabbits were injected simultaneously with both low- and high-affinity bisphosphonate analogs and then skeletal distribution at the BMU level was assessed using confocal microscopy.

Materials and Methods

Animals

Skeletally mature female New Zealand white rabbits (9 months old, $n = 8$) were obtained from Myrtle's Rabbitry (Thompson Station, TN). Rabbits were used for this study as they, unlike rodents, have haversian systems and, therefore, a cortical bone vascular pattern similar to that of humans. Animals were housed individually at the Indiana University animal care facility and had ad libitum access to food and water. Prior to the study, all protocols were approved by Indiana University School of Medicine Institutional Animal Care and Use Committee.

Synthesis and Purification of Fluorescent Probes

RIS was kindly provided by Warner Chilcott Pharmaceuticals (Dundalk, Ireland). 5(6)-X-Rhodamine succinimidyl ester (SE) and Alexa Fluor 647 SE were purchased from Invitrogen (Carlsbad, CA). The high-affinity compound AF647-RIS was synthesized by direct reaction between RIS and the linker in aqueous alcohol, followed by linker deprotection and conjugation with the activated dye, and then purified and characterized

as described previously [10, 14]. The low-affinity compound, a phosphonocarboxylate (ROX-3-PEHPC), was synthesized similarly using a rhodamine-2 fluorophore. Previous work has shown that phosphonocarboxylates, which substitute one phosphonate group of a bisphosphonate with a carboxylate group, are functional analogs of traditional bisphosphonates yet have lower mineral binding affinity [2]. The specific phosphonocarboxylate used in this study has a 50% lower mineral binding affinity compared to the parent RIS compound, determined using a hydroxyapatite column binding assay. The addition of fluorescent tags has been shown to reduce bone affinity by about 25% relative to the parent compound [5, 10]. All probes had satisfactory ^1H and ^{31}P NMR spectra, LC-MS and HRMS, and emission and absorption spectra and were >98% pure by HPLC.

Experimental Design

Following 1 week of acclimatization at the Indiana University School of Medicine, animals were randomly assigned to two groups ($n = 4/\text{group}$). One group was fed a low-calcium diet (Harlan Teklad, Madison, WI; TD.87370, 0.1% calcium) in order to stimulate bone turnover [15]. The second group was fed a normal-calcium diet (Harlan Teklad Global Rabbit Diet 2030, 0.89% calcium). As dynamic histomorphometric measures revealed no difference in remodeling rate between these two groups (Table 1), all animals were pooled together for analyses.

After 8 weeks on the diet, a duration corresponding to roughly two remodeling cycles in a rabbit [16], animals were injected intramuscularly with calcein (10 mg/kg dose at a concentration of 20 mg/ml) to label actively forming bone surfaces; a second injection of calcein was administered 10 days later. One week after the second calcein injection, all animals were given simultaneous intravenous injections of two different fluorescent bisphosphonate analogs. Agents were dissolved in phosphate-buffered saline and administered at a dose of 3 μg phosphorus/kg body weight [5]. As a control, two additional rabbits, fed a normal-calcium diet, were treated as described above with compounds labeled with the opposite fluorophore (AF647 on the low-affinity compound and rhodamine-2 on the high-affinity compound) to qualitatively determine if the specific fluorophore had an effect on the imaging properties or penetration depth characteristics.

Twenty-four hours after dosing of the bisphosphonate analogs, animals were killed by intravenous injection of a lethal dose of sodium pentobarbital. The rib, tibia diaphysis, and third lumbar vertebra were dissected free and placed in 10% neutral buffered formalin for 24 h and then switched to 70% ethanol. The rib and tibia were used as cortical bone sites with high and low basal turnover, respectively. The vertebra was used as a trabecular bone site of clinical relevance.

Tissue Processing

Bones were embedded in methyl methacrylate using a standard protocol [17]. The rib and tibia were sectioned in the transverse plane using a diamond wire saw and then hand-ground to a final thickness of $\sim 50 \mu\text{m}$. Lumbar vertebrae were sectioned (8 μm thickness) in the sagittal plane using a rotary microtome. All slides were coverslipped using a nonfluorescent mounting medium (Eukitt; Kindler, Freiburg, Germany).

Confocal Microscopy

Bone sections were examined using an Olympus (Tokyo, Japan) FV-1000 confocal microscope with a 60× oil immersion lens (Fig. 1). Fluorescence intensity from each channel (calcein, rhodamine-2, and AF647) was optimized for black level without any oversaturated pixels. Excitation wavelengths for calcein, rhodamine-2, and AF647 were 488, 539, and 635 nm, respectively. Emission spectra collection ranges were adjusted around the emission peaks of 520 nm (calcein), 577 nm (rhodamine-2), and 688 nm (AF647) to provide the maximal signal intensity with minimal channel cross-talk. Image Z stacks (1 μm optical thickness) of 10–12 image planes (rib and tibia) and 5–8 image planes (lumbar vertebrae) were collected sequentially with only one laser on per fluorophore. Image stacks from three double calcein-labeled osteons in the cortical bone of the rib and tibia or hemi osteons in the trabecular bone of lumbar vertebrae were collected from each animal. Hemi osteons in lumbar vertebrae were identified by collagen fiber orientation using brightfield polarized light.

Image Analysis

Images were exported as 24-bit composite RGB TIFF files using the Olympus FV-10-ASW viewer software. ImageJ (National Institutes of Health, Bethesda MD) was used for all subsequent image analyses [18]. A maximum intensity Z projection of each image stack was made, and the red (AF647-HIGH) and blue (RHOD2-LOW) channels were separated. The lookup table was inverted so that stained regions were dark upon a light-colored background. A brightfield image was used to identify the osteon cement line or hemi osteon structure, and this image was synchronized with the red and blue channel windows so that tracings on one image were identically traced in other windows.

Stained regions around osteocytes were traced (Fig. 2), and the staining intensity was determined using the mean gray-scale value of all pixels outlined. All osteocytes were traced in two areas: (1) those within the osteon/hemi osteon and (2) those within a 100 μm distance outside the structure. For both high and low compounds, the average gray-scale value (osteocyte staining) of all osteocytes within the cement line was compared to the same number of osteocytes outside the cement line to provide a staining intensity ratio. This method of analysis was chosen as it allows each image to serve as its own control and removes variation of staining intensity between the different fluorophores as a factor in the analysis. At each skeletal site data from the individual osteons were summed, and those values were used to calculate ratios.

Dynamic Histomorphometry

Dynamic histomorphometric measurements were made on the tibia, rib, and vertebrae using a Nikon (Tokyo, Japan) Optiphot 2 fluorescent microscope and Bioquant image analysis system (R&M Biometrics, Nashville, TN). For vertebrae, mineralizing surface/bone surface (MS/BS)— $\{[\text{double label surface} + (0.5 * \text{single label surface})]/\text{bone surface}\} \times 100$ —mineral apposition rate (MAR)—distance between calcein labels/days between sets of labels—and bone formation rate (BFR/BS)— $\text{MAR} * (\text{MS/BS}/100) * 365$ —were collected using standard methods as previously described [17]. For rib and tibia diaphysis, intracortical measures of MAR and bone formation rate (BFR/B.Ar)— $\text{MAR} * [(\text{labeled}$

surface/2)/cortical bone area] *365—were determined [19]. Two histological sections were analyzed for each animal at each region.

Statistics

All statistical tests were run using GraphPad (San Diego, CA) Prism software. The effects of calcium restriction and between-staining ratios were assessed using Mann-Whitney and Wilcoxon nonparametric tests. $P < 0.05$ was considered statistically significant.

Results

Effect of Calcium Restriction on Bone Turnover Rate

Following 8 weeks of calcium restriction, bone remodeling was not significantly altered in any of the skeletal sites assessed (Table 1). Therefore, the two groups of animals were pooled for all analyses.

Fluorescent Bisphosphonate Localization in Cortical Bone

Qualitative observations in the rib revealed that the low- and high-affinity compounds labeled the endocortical surface and the bone surrounding the haversian canals with high intensity, while the canaliculi and osteocyte lacunae were labeled to a lesser degree (Fig. 2). Endocortical surfaces and haversian canals were routinely observed to have two bands of fluorescence, with the low-affinity drug slightly deeper in the matrix compared to the higher-affinity drug (Fig. 1). This was likely due to the fact that the low-affinity drug penetrated deeper into the matrix compared to the higher-affinity drug, consistent with previous reports using two different-affinity compounds [7, 8]. In control animals that were dosed with agents having flipped fluorophores, the qualitative banding pattern was reversed, indicating that the banding was not a function of the fluorophore but rather a function of the binding affinity of the drug (Fig. 3).

Quantitatively, the staining intensity ratio between osteocytes contained within the cement line of newly formed rib osteons compared to osteocytes outside the cement line was higher for the high-affinity drug compared to the low-affinity drug (Fig. 4a). This indicates that the low-affinity drug distributes more equally across the osteonal cement line compared to the high-affinity drug, which concentrates mostly within the osteonal structure. Staining intensity ratios were calculated in the ribs of the two animals with the flipped fluorophores, and although the pattern was similar, the data were not significantly different (high affinity 1.50 ± 0.17 , low affinity 1.20 ± 0.06). In tibial osteons the staining of the two fluorophores was almost exclusively within the cement lines of the forming osteons. Therefore, ratios of staining were not possible to calculate.

Fluorescent Bisphosphonate Localization in Trabecular Bone

Qualitative observations on cancellous bone surfaces showed a similar banding pattern as was noted in cortical surfaces (Fig. 5). Similar to the rib, there was a significantly lower ratio of the low-affinity compound compared to the high-affinity compound (Fig. 4b).

Discussion

The ability of bisphosphonates to bind to hydroxyapatite has been long appreciated [20], yet the details of this physical–chemical interaction have been elucidated only recently. We know that bisphosphonates have different binding affinities that contribute to the adsorption and release from mineral [1, 3]. We also have begun to learn how binding affinity affects the global and tissue-level distribution of bisphosphonates [4–6]. Previous work on skeletal distribution has predominantly focused on trabecular bone as this is where bisphosphonates produce their most prominent skeletal effect. Yet bisphosphonates also significantly benefit cortical bone by reducing porosity through suppression of intracortical remodeling [21–24]. Rodents represent a useful model for studying trabecular bone but have significant limitations in cortical bone studies due to their lack of intracortical remodeling. The goal of the current work was to determine whether differences in bisphosphonate binding affinity affected distribution in cortical and cancellous bone. Our results show that within the cortical bone of the rib compounds with high affinity are mostly localized within the osteonal units while those with lower affinities have a greater ability to diffuse beyond the osteonal cement line. These results differed in the tibia, where neither the high- nor the low-affinity drug was detected beyond the osteonal cement line.

Fluorescently labeled bisphosphonates with different binding affinities provide unique tools to study drug distribution [7–9]. Phosphonocarboxylates are functional analogs to traditional bisphosphonate yet have mineral binding affinities that are about half that of the parent compound based on in vitro column binding assays [2]. After completion of the in vivo experiments, in vitro binding assays were conducted on the specific compounds used in these studies. The results were unexpected, showing that the two compounds used in the main study (phosphonocarboxylate attached to rhodamine and RIS attached to AF647) could not be differentiated with respect to binding affinities. The assay was able to differentiate the compounds used in the second experiment, showing that the phosphonocarboxylate combined with an Alexa Fluor tag had a binding affinity that was 75% lower than the RIS combined with rhodamine. The explanation for the lack of a binding affinity difference between the two main compounds using our in vitro assay is unclear. Our in vivo data strongly suggest differences in affinity as the distribution results match recent work in which compounds with quantifiable differences in affinity by in vitro assay show differences in distribution from the bone surface in rats [9]. Furthermore, in the current work there is strong consistency between the first and second experiments, the latter using compounds with confirmed differences in affinity by in vitro assay. One explanation is that the in vitro assay simply did not capture some feature of the in vivo system for these particular compounds/fluorophore combinations. For example, the in vitro experiment runs the compounds through a column of hydroxyapatite, while the in vivo experiment examines how the agents travel through the vasculature and lacuna/canalicular system before binding to a free surface. The in vitro assay is also done with pure hydroxyapatite and, thus, lacks the collagen and noncollagenous proteins that exist in vivo.

The clinical implications of differences in binding affinity and, more specifically, differences in skeletal distribution remain speculative, although mounting indirect evidence suggests a number of plausible effects. Bisphosphonates reduce osteocyte apoptosis [13]. This has

been suggested to have independent positive effects on bone mechanical properties [25]. Those cells most susceptible to apoptosis reside in the interstitial bone that is located farthest from a bone surface or vascular space. Our findings suggest that, at least in some bones, bisphosphonates with lower binding affinities have a greater capacity to reach these areas deep in the bone, where the most vulnerable osteocytes reside. Even without affecting osteocytes, a more widespread distribution of drug throughout the cortex could provide a more uniform reduction in remodeling. This idea is supported by clinical evidence showing that a bisphosphonate with lower relative binding affinity (e.g., RIS relative to alendronate) produces a more rapid reduction in fracture risk [3, 26]. As it is difficult to directly relate the binding affinity of these fluorescent compounds to native compounds, it is unclear to what degree a traditional bisphosphonate would penetrate across the cement line to the interstitial bone.

Our analyses show similar patterns of skeletal distribution between the low- and high-affinity compounds in both rib cortical and vertebral trabecular bone, while the tibial cortex showed different results. Drug distribution to the trabecular bone is likely dictated by the amount of drug that enters the marrow cavity through sinusoidal capillaries. Once entering the marrow, the drug's affinity for mineral drives it toward trabecular surfaces, where it either binds or diffuses into the canalicular network until becoming bound. Few areas of human trabecular bone are beyond 100 μm from any given surface [27, 28]. This makes most regions of trabecular bone accessible to even high-affinity bisphosphonates. Nonetheless, our data, as well as those from others [7, 8], show that a lower-affinity drug can penetrate deeper relative to a given surface compared to a higher-affinity drug. Conversely, a significant portion of cortical bone is in the form of interstitial bone, which in many cases is more than 100 μm from a vascular surface and may be relatively inaccessible to bisphosphonates.

It was not possible to measure staining intensity in the tibial cortex due to a paucity of fluorescent compound passing beyond the cement line. The tibia has a much lower metabolic need and lower perfusion [29–31] due to lower rates of remodeling compared to the rib (1% compared to 50%). A lower relative blood flow would mean a smaller amount of drug available for diffusion into a given osteon. Additionally, the lower remodeling rate of the tibia likely results in a higher interstitial bone mineral content (relative to interstitial bone in the rib), which may affect diffusion beyond the cement line.

Our study utilized a single dose of each bisphosphonate analog in order to simplify the interpretation and because of a finite amount of fluorescent compound. It is possible that repeated administration of drug, similar to what is done clinically, could alter the distribution of drug. However, repeated dosing is unlikely to saturate the surfaces and thus “force” a given compound deeper into the matrix. Previous unpublished work has used doses 10 times higher than those used in the current study and found a significant amount of bone surface having colocalization of both high- and low-affinity compounds, suggesting saturation would not occur even at those doses.

The ability to view two different drug analogs within the same animal has significant advantages as it is possible to make direct comparisons between agents without having

to account for differences among animals. Yet this study design also presents technical challenges and limitations. In order to clearly observe each fluorophore, the confocal laser/camera settings were separately optimized. This makes direct comparisons of raw pixel staining between fluorophores inappropriate and resulted in our decision to normalize the distribution of each fluorophore to itself and focus on regions of skeletal distribution. As such, we cannot draw conclusions about the relative amounts of each agent and how these may differ between the low- and high-affinity compounds at a given location or even within a given affinity across skeletal sites.

In conclusion, we show that mineral binding affinity significantly affects the distribution of bisphosphonates around forming cortical bone osteons in the rib and trabecular hemiosteons of the vertebrae but not cortical bone of the tibial diaphysis. These data, from an animal model that undergoes intracortical remodeling similar to humans, provide some insight into how various bisphosphonates may be differentially distributed in cortical bone.

Acknowledgement

The authors thank the following individuals for their technical contributions to the project: Dr. Keith Condon (tissue processing), Drs. Malgorzata Kamocka and Ken Dunn (technical assistance with confocal microscopy set-up), and Carrie Pell and staff (animal care/dosing). The confocal microscopy was performed within the Indiana Center for Biological Microscopy Resources. Funding for this study was provided by a grant from Warner Chilcott.

References

1. Nancollas GH, Tang R, Phipps RJ, Henneman Z, Gulde S, Wu W, Mangood A, Russell RG, Ebetino FH (2006) Novel insights into actions of bisphosphonates on bone: differences in interactions with hydroxyapatite. *Bone* 38:617–627 [PubMed: 16046206]
2. Ebetino FH, Hogan A-ML, Sun S, Tsoumpra MK, Duan X, Triffitt JT, Kwaasi AA, Dunford JE, Barnett BL, Oppermann U, Lundy MW, Boyde A, Kashemirov BA, McKenna CE, Russell RGG (2011) The relationship between the chemistry and biological activity of the bisphosphonates. *Bone* 49:20–33 [PubMed: 21497677]
3. Russell RG, Watts NB, Ebetino FH, Rogers MJ (2008) Mechanisms of action of bisphosphonates: similarities and differences and their potential influence on clinical efficacy. *Osteoporos Int* 19:733–759 [PubMed: 18214569]
4. Sato M, Grasser W, Endo N, Akins R, Simmons H, Thompson DD, Golub E, Rodan GA (1991) Bisphosphonate action. Alendronate localization in rat bone and effects on osteoclast ultrastructure. *J Clin Invest* 88:2095–2105 [PubMed: 1661297]
5. Roelofs AJ, Coxon FP, Ebetino FH, Lundy MW, Henneman ZJ, Nancollas GH, Sun S, Blazewska KM, Lynn FBJ, Kashemirov BA, Khalid AB, McKenna CE, Rogers MJ (2009) Fluorescent risedronate analogs reveal bisphosphonate uptake by bone marrow monocytes and localization around osteocytes in vivo. *J Bone Miner Res* 25:606–616
6. Kozloff KM, Volakis LI, Marini JC, Caird MS (2010) Near-infrared fluorescent probe traces bisphosphonate delivery and retention in vivo. *J Bone Miner Res* 25:1748–1758 [PubMed: 20200982]
7. Roelofs AJ, Boyde A, Lundy MW, McKenna CE, Blazewska K, Sun ST, Kashemirov BA, Russell RGG, Ebetino FH, Rogers MJ, Coxon FP (2009) Bone mineral affinity influences the distribution of a bisphosphonate and a lower affinity analogue in vivo. *Bone* 44:S430–S431
8. Boyde A, Lundy MW, Coxon FP, McKenna CE, Roelofs A, Bala J, Rogers MJ, Blazewska K, Russell RGG, Ebetino FH (2009) The differential distribution in vivo of fluorescently-labeled bisphosphonate analogues with different mineral affinity to bone surfaces. *Bone* 44:S57

9. Roelofs A, Stewart CA, Sun S, Blazewska K, Kashemirov BA, McKenna CE, Russell RGG, Rogers MJ, Lundy MW, Ebetino FH, Coxon FP (2011) Influence of bone affinity on the skeletal distribution of fluorescently-labeled bisphosphonates in vivo. *J Bone Miner Res* (in press)
10. Kashemirov BA, Bala JLF, Chen X, Ebetino F, Xia Z, Russell RGG, Coxon FP, Roelofs AJ, Rogers MJ, McKenna CE (2008) Fluorescently labeled risedronate and related analogues: magic linker synthesis. *Bioconjug Chem* 19:2308–2310 [PubMed: 19032080]
11. Liu H, Ren G, Miao Z, Zhang X, Tang X, Han P, Gambhir SS, Cheng Z, Boswell A (2010) Molecular optical imaging with radioactive probes. *PLoS One* 5:e9470 [PubMed: 20208993]
12. Plotkin LI, Aguirre JI, Kousteni S, Manolagas SC, Bellido T (2005) Bisphosphonates and estrogens inhibit osteocyte apoptosis via distinct molecular mechanisms downstream of extracellular signal-regulated kinase activation. *J Biol Chem* 280:7317–7325 [PubMed: 15590626]
13. Plotkin LI, Weinstein RS, Parfitt AM, Roberson PK, Manolagas SC, Bellido T (1999) Prevention of osteocyte and osteoblast apoptosis by bisphosphonates and calcitonin. *J Clin Invest* 104:1363–1374 [PubMed: 10562298]
14. Sun S, Blazewska KM, Kashemirov BA, Roelofs AJ, Coxon FP, Rogers MJ, Ebetino FH, McKenna MJ, McKenna CE (2011) Synthesis and characterization of novel fluorescent nitrogen-containing bisphosphonate imaging probes for bone active drugs. *Phosphorus Sulfur Silicon Relat Elem* 186:970–971 [PubMed: 21894242]
15. Wu D, Boyd R, Fix T, Burr DB (1990) Regional patterns of bone loss and altered bone remodeling in response to calcium deprivation in laboratory rabbits. *Calcif Tissue Int* 47:18–23 [PubMed: 2369687]
16. Mashiba T, Burr DB, Turner CH, Sato M, Cain RL, Hock JM (2001) Effects of human parathyroid hormone (1–34), LY333334, on bone mass, remodeling, and mechanical properties of cortical bone during the first remodeling cycle in rabbits. *Bone* 28:538–547 [PubMed: 11344054]
17. Allen MR, Iwata K, Phipps R, Burr DB (2006) Alterations in canine vertebral bone turnover, microdamage accumulation, and biomechanical properties following 1-year treatment with clinical treatment doses of risedronate or alendronate. *Bone* 39:872–879 [PubMed: 16765660]
18. Abramoff MD, Magalhaes P, Ram S (2004) Image processing with ImageJ. *Biophoton Int* 11:36–43
19. Allen MR, Kubek DJ, Burr DB (2010) Cancer treatment dosing regimens of zoledronic acid result in near-complete suppression of mandible intracortical bone remodeling in beagle dogs. *J Bone Miner Res* 25:98–105 [PubMed: 19580463]
20. Fleisch H, Russell RGG, Francis MD (1969) Diphosphonates inhibit hydroxyapatite dissolution in vitro and bone resorption in tissue culture and in vivo. *Science* 165:1262 [PubMed: 5803538]
21. Borah B, Dufresne T, Nurre J, Phipps R, Chmielewski P, Wagner L, Lundy M, Bouxsein M, Zebaze R, Seeman E (2010) Risedronate reduces intracortical porosity in women with osteoporosis. *J Bone Miner Res* 25:41–47 [PubMed: 19580469]
22. Roschger P, Rinnerthaler S, Yates J, Rodan GA, Fratzl P, Klaushofer K (2001) Alendronate increases degree and uniformity of mineralization in cancellous bone and decreases the porosity in cortical bone of osteoporotic women. *Bone* 29:185–191 [PubMed: 11502482]
23. Allen MR, Reinwald S, Burr DB (2008) Alendronate reduces bone toughness of ribs without significantly increasing microdamage accumulation in dogs following 3 years of daily treatment. *Calcif Tissue Int* 82:354–360 [PubMed: 18463913]
24. Smith SY, Recker RR, Hannan M, Muller R, Bauss F (2003) Intermittent intravenous administration of the bisphosphonate ibandronate prevents bone loss and maintains bone strength and quality in ovariectomized cynomolgus monkeys. *Bone* 32:45–55 [PubMed: 12584035]
25. Bellido T, Plotkin LI (2011) Novel actions of bisphosphonates in bone: preservation of osteoblast and osteocyte viability. *Bone* 49:50–55 [PubMed: 20727997]
26. Silverman SL, Watts NB, Delmas PD, Lange JL, Lindsay R (2007) Effectiveness of bisphosphonates on nonvertebral and hip fractures in the first year of therapy: the risedronate and alendronate (REAL) cohort study. *Osteoporos Int* 18:25–34 [PubMed: 17106785]
27. Khosla S, Riggs BL, Atkinson EJ, Oberg AL, McDaniel LJ, Holets M, Peterson JM, Melton LJ III (2006) Effects of sex and age on bone microstructure at the ultradistal radius: a population based noninvasive in vivo assessment. *J Bone Miner Res* 21:124–131 [PubMed: 16355281]

28. Recker RR, Kimmel DB, Parfitt MA, Davies MK, Keshawarz N, Hinders S (1988) Static and tetracycline based bone histomorphometric data from 34 normal postmenopausal females. *J Bone Miner Res* 3:133–144 [PubMed: 3213608]
29. Sim FH, Kelly P (1970) Relationship of bone remodeling, oxygen consumption, and blood flow in bone. *J Bone Joint Surg* 52:1377 [PubMed: 5469192]
30. Morris MA, Kelly PJ (1980) Use of tracer microspheres to measure bone blood flow in conscious dogs. *Calcif Tissue Int* 32:69–76 [PubMed: 6775781]
31. Whiteside LA, Simmons DJ, Lesker PA (1977) Comparison of regional bone blood flow in areas with differing osteoblastic activity in the rabbit tibia. *Clin Orthop Relat Res* 124:267

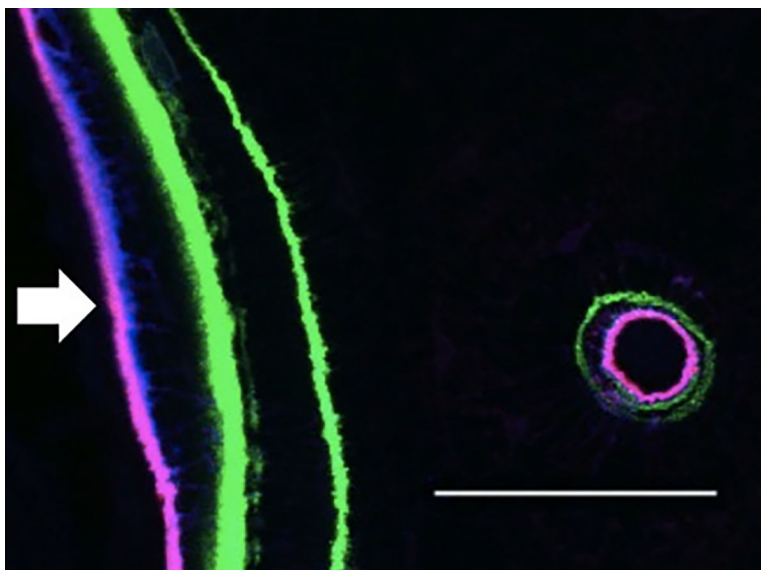


Fig. 1. Maximum-intensity projection of confocal image stack showing a double calcein label (*green*) at a remodeling site on the endocortical surface of the rib (*arrow*). A single labeled osteon can also be seen nearby. The fluorescent agents can be observed near the endocortical surface and the bone adjacent to the Haversian canal. *Blue* (RHOD2 low-affinity compound) staining penetrates farther into the bone at the endocortical surface. *Magenta* is a combination of the high-affinity (AF647-HIGH) and low-affinity (RHOD2-LOW) agents colocalized at a given site (bar = 50 μm)

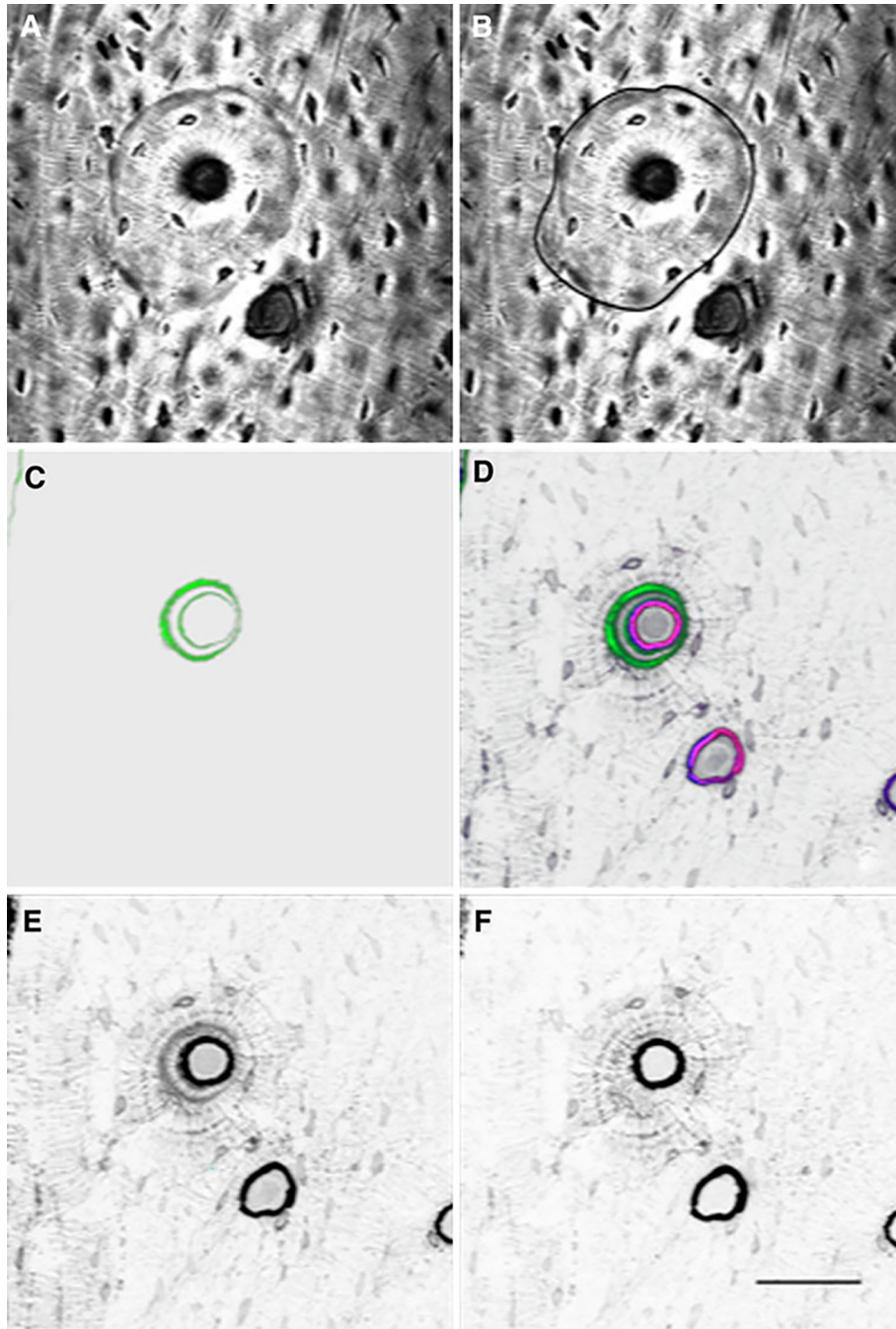


Fig. 2. A typical osteon within the rib cortex that was analyzed for drug distribution. **a** Brightfield image of the osteon used to identify the cement line that defines the outer boundary. **b** Brightfield image of the osteon depicting the tracing of the cement line for analyses. **c** 3D image reconstruction showing calcein labeling (*green pseudocolor*). **d** 3D image reconstruction of image stack showing calcein labeling and both fluorescent bisphosphonate stains of bone adjacent to the haversian canals, canaliculi, and osteocytes. *Green pseudocolor* represents calcein, *blue* represents RHOD2-LOW staining, *red* represents

AF647-HIGH staining, and *magenta* represents the combination of RHOD2 and AF647 colocalization. **e** Isolation of RHOD2 channel showing localization of the low-affinity drug (no pseudocolor, *dark pixels* indicate regions of drug binding) independent of all other fluorophores. **f** Isolation of AF647 channel showing localization of the high-affinity drug (no pseudocolor, *dark pixels* indicate regions of drug binding) independent of all other fluorophores (bar = 50 μ m). The greater number of *darker pixels* in **e** than **f** shows that the low-affinity bisphosphonate is distributing more deeply into the tissue than the higher-affinity bisphosphonate

Author Manuscript

Author Manuscript

Author Manuscript

Author Manuscript

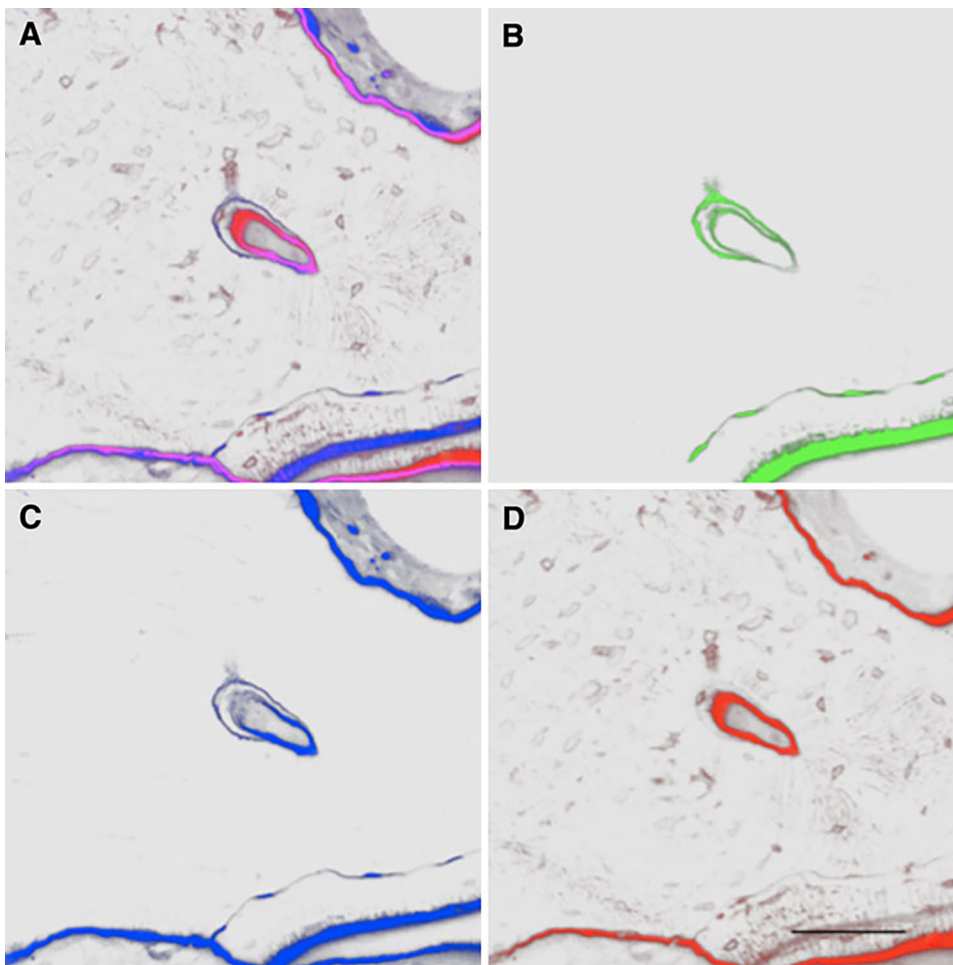


Fig. 3. A representative osteon within the rib cortex of an animal labeled with the opposite fluorophores of the main experiment (AF647 on the low-affinity compound and Rhod2 on the high-affinity compound). **a** 3D image reconstruction of image stack showing labeling of both fluorescent bisphosphonate stains of bone adjacent to the haversian canals, canaliculi, and osteocytes. Portions of the endocortical surface can also be observed. *Blue pseudocolor* represents RHOD2-HIGH staining, *red* represents AF647-LOW staining, and *magenta* represents the combination of RHOD2 and AF647 colocalization. **b** 3D image reconstruction showing calcein labeling (*green pseudocolor*). **c** Isolation of RHOD2 channel showing localization of the high-affinity drug (*blue pseudocolor*, *dark pixels* indicate regions of drug binding) independent of all other fluorophores. **d** Isolation of AF647 channel showing localization of the low-affinity drug (*red pseudocolor*, *dark pixels* indicate regions of drug binding) independent of all other fluorophores (bar = 50 μm). The greater number of *darker pixels* in **d** than **c** shows that the low-affinity bisphosphonate is distributing more deeply into the tissue than the higher-affinity bisphosphonate

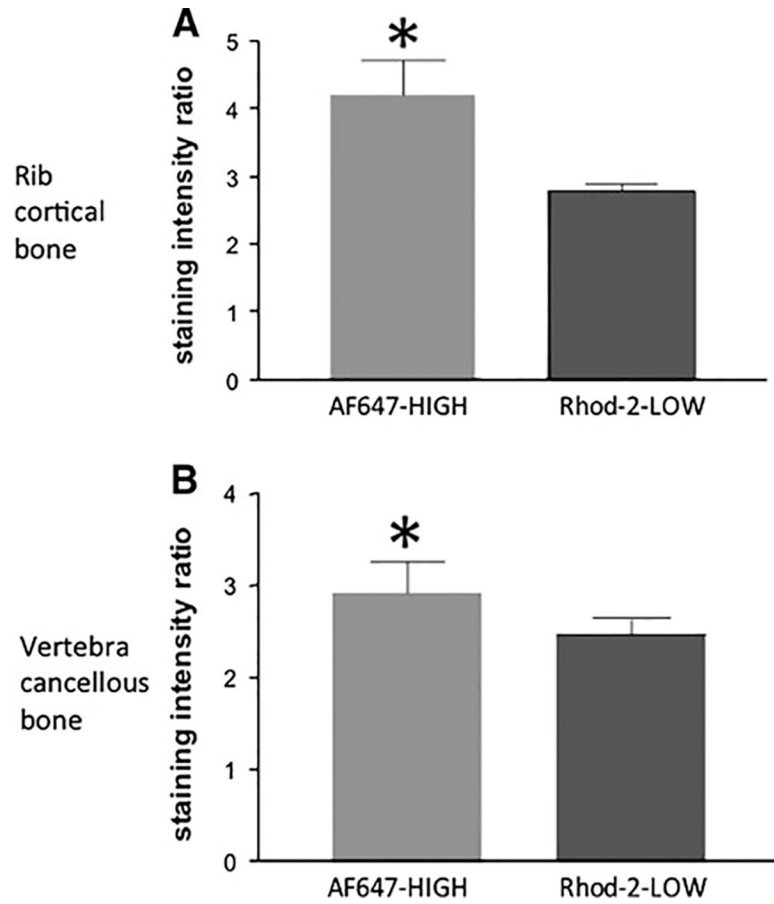


Fig. 4. Staining intensity ratio in cortical bone of the rib (**a**) and trabecular bone of the vertebra (**b**). Data represent the ratio of stained osteocytes within the cement/reversal line of a remodeling unit to those outside that boundary in interstitial bone ($n = 8$ animals). Having a higher ratio indicates that a smaller amount of drug crosses the boundary out into the interstitial bone. * $P < 0.05$

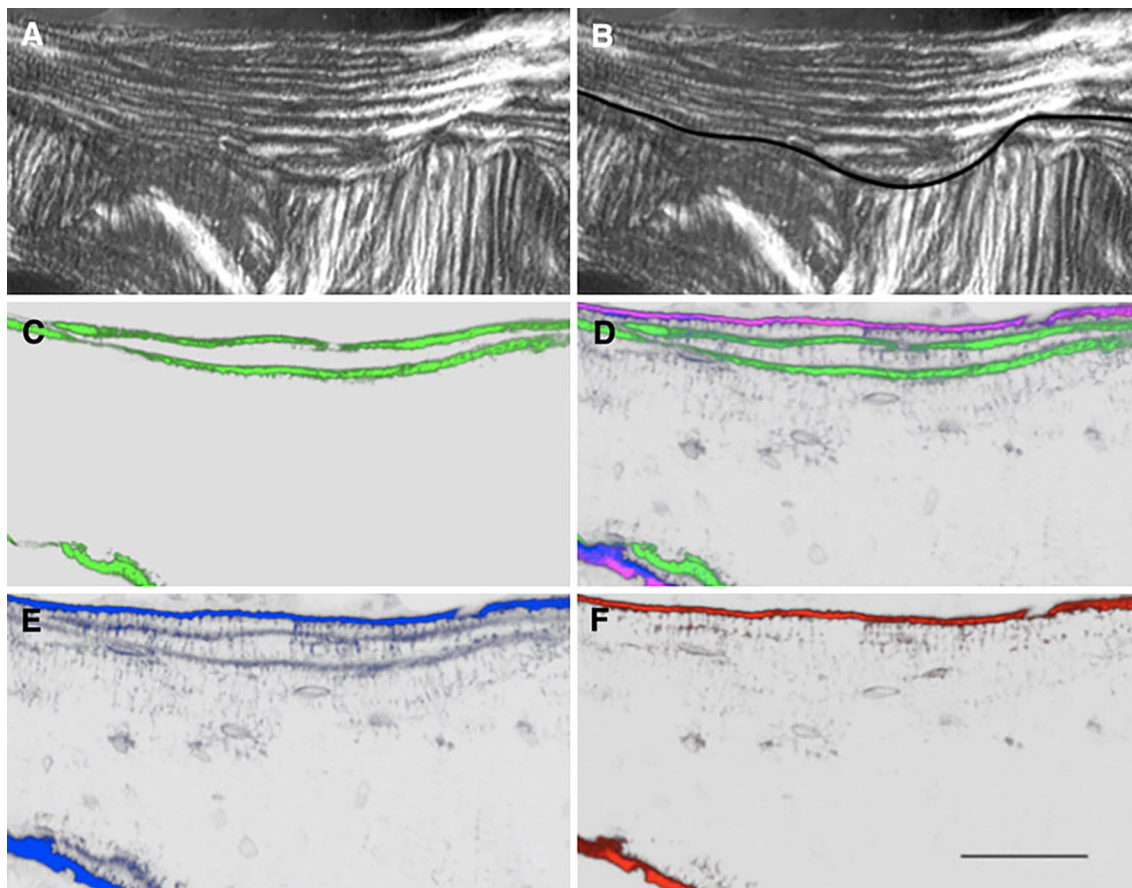


Fig. 5. Lumbar vertebrae cancellous bone section. **a** Polarized light image showing hemiosteon (*arrow*). **b** Polarized light image of the hemiosteon depicting the tracing of the cement line for analyses. **c** 3D image reconstruction showing calcein labeling (*green pseudocolor*). **d** 3D image reconstruction of image stack showing calcein labeling and fluorescent bisphosphonate staining of bone near surfaces. *Green pseudocolor* represents calcein, *blue* represents RHOD2-LOW staining, *red* represents AF647-HIGH staining, and *magenta* represents the combination of RHOD2 and AF647 colocalization. **e** Isolation of RHOD2 channel showing (*blue pseudocolor*) localization of the low-affinity drug independent of all other fluorophores. **f** Isolation of AF647 channel showing (*red pseudocolor*) localization of the high-affinity drug independent of all other fluorophores (bar = 50 μm)

Table 1

Effects of calcium restriction on cortical and trabecular bone remodeling

	Low-calcium diet (<i>n</i> = 4)	Normal-calcium diet (<i>n</i> = 4)	<i>P</i>
Tibia			
MAR (μm)	2.24 \pm 0.71	1.58 \pm 1.01	0.39
BFR (%/year)	8.54 \pm 4.99	1.19 \pm 1.07	0.08
Rib			
MAR (μm)	1.44 \pm 0.32	1.64 \pm 0.41	0.15
BFR (%/year)	37.55 \pm 9.84	50.30 \pm 23.5	0.25
Vertebra			
MAR (μm)	2.27 \pm 0.34	2.39 \pm 0.17	0.77
MS/BS (%)	42.6 \pm 13.6	31.2 \pm 3.33	0.25
BFR ($\mu\text{m}^3/\mu\text{m}^2/\text{year}$)	99.8 \pm 41.2	74.6 \pm 11.3	0.25

Data are presented as mean \pm standard deviation*MAR* mineral apposition rate, *BFR* bone formation rate, *MS/BS* mineralizing surface per unit bone surface*P* values from Mann–Whitney nonparametric tests